J Solid State Electrochem (2010) 14:659–668
DOI 10.1007/s10008-009-0816-3

ORIGINAL PAPER

Electrochemical kinetic study about cobalt electrodeposition onto GCE and HOPG substrates from sulfate sodium solutions

C. H. Rios-Reyes · L. H. Mendoza-Huizar · M. Rivera

Received: 27 January 2009 / Revised: 22 February 2009 / Accepted: 22 February 2009 / Published online: 4 April 2009

Abstract In the present work, we analyze the electrodeposition of cobalt by electrochemical techniques onto GCE (system I) and HOPG (system II) electrodes from sulfate solutions. Cyclic voltammetry and current transient measurements were used to obtain the nucleation and growth mechanism. The results clearly showed that electrodeposition of cobalt is a diffusion-controlled process with a typical 3D nucleation mechanism in both substrates. The average ΔG calculated for the stable nucleus formation was 1.97×10^{-20} J nuclei^{-1} and 3.58×10^{-20} J nuclei^{-1} for system I and system II, respectively. The scanning electron microscope (SEM) images indicated similar nucleation and growth processes on GCE and HOPG substrates at same overpotential with a homogeneous disperse cobalt clusters. X-ray energy-dispersive spectroscopy (EDS) was performed in order to ensure that the clusters formed are cobalt. The nuclei's size obtained was dependent of the overpotential applied; at lower overpotentials, the growth rate of the cobalt clusters diminishes when their number increases due to the strongly reduced concentration of cobalt ions because of their consumption by a larger number of growing particles. A theoretical quantum study employing PM6 method suggests that Na^+ adsorbed deactivate the local surface occasionating the formation of disperse cobalt clusters on carbon electrodes.

Keywords Cobalt · Nucleation · Sulfate · GCE · HOPG · PM6

C. H. Rios-Reyes · L. H. Mendoza-Huizar
Centro de Investigaciones Químicas,
Universidad Autónoma del Estado de Hidalgo,
Mineral de la Reforma,
Hidalgo C.P. 42186, México

C. H. Rios-Reyes
Departamento de Materiales,
Universidad Autónoma Metropolitana-Azcapotzalco,
Av. San Pablo 180, Col. Reynosa Tamaulipas,
C.P. 02200 México D.F., México

M. Rivera
Instituto de Física, Dpto. Materia Condensada,
Universidad Nacional Autónoma de México,
Ciudad Universitaria, Coyoacán,
C.P. 04510 México D.F., México

L. H. Mendoza-Huizar (✉)
Centro de Investigaciones Químicas,
Universidad Autónoma del Estado de Hidalgo,
Carretera Pachuca-Tulancingo km. 4.5, Mineral de la Reforma,
Hidalgo, México
e-mail: hhuizar@uaeh.edu.mx

Introduction

Electrodeposited cobalt and cobalt alloys are widely employed throughout the computer industry as the recording media in both magnetic drum and magnetic tape memory systems [1, 2]. Cobalt electrodeposition studies can be categorized according to the working electrode and the type of solution system employed [3, 4]. However, most of the studies have been performed onto glassy carbon electrodes [5–10]. Chloride solutions have been the preferred systems for studying the electrochemistry of cobalt [8–12], rather than sulfate systems [6, 13, 14] or citrate solutions [4]. In summary, it has been found that cobalt electrodeposition predominantly initiates through progressive nucleation, which can change to instantaneous nucleation mechanisms by enhancing mass transfer, using ultrasound [6], or increasing cobalt concentration [9]. However, the electrodeposition of cobalt may occur

through a nucleation process under charge transfer control too [15].

Sulfate baths have been few used probably due to that the sulfate anion induces a competitive adsorption effect on the substrate complicating the electrodeposition process [16, 17]. On the other hand, Na^+ ions do not react electrochemically at the electrode surface allowing a major control on the electrodeposition. Recent results on the growth of cobalt clusters onto HOPG electrodes from sodium sulfate solutions support these observations [18]. However, a kinetic study of the electrodeposition process of cobalt onto carbon electrodes from sodium sulfate solutions is missing. Thus, in order to understand this process, we study the kinetic of cobalt electrodeposition onto HOPG and GCE electrodes. We compare the results obtained in order to analyze the influence of the carbon surface in the cobalt electrodeposition process.

Methodology

Experimental

Cobalt electrodeposits onto glassy carbon (GCE) and high oriented pyrolytic graphite (HOPG) electrodes were carried out from an aqueous solution containing 10^{-2}M of $CoSO_4$ +1 M Na_2SO_4 at pH=7.1 (natural pH). All solutions were prepared using analytic grade reagents with ultra pure water (Millipore-Q system) and were deoxygenated by bubbling N_2 for 15 min before each experiment. The working electrodes were a GCE tip provided by BAS™, with 0.071 cm^2 and freshly cleaved HOPG surfaces. In the case of GCE, the exposed surface was polished to a mirror finish with different grades of alumina down to 0.05 μm and ultrasonically cleaned before experiments. A graphite bar with an exposed area greater than the working electrode was used as counter electrode. A saturated silver electrode (Ag/AgCl) was used as the reference electrode, and all measured potentials are referred to this scale. All experiments were carried out at 25 °C. The electrochemical experiments were carried out in a BAS potentiostat connected to a personal computer running the BAS100W software to allow control of experiments and data acquisition. In order to verify the electrochemical behavior of the electrode in the electrodeposition bath, cyclic voltammetry was performed in the 0.600 to −1.200 V potential range. The kinetic mechanism of cobalt deposit onto GCE was studied under potentiostatic conditions by means of the analysis of the experimental current density transients obtained with the potential step technique. The perturbation of the potential electrode always started at 0.600 V. The potential step was imposed at different potentials detailed in this work. Microstructures of electrodeposits were examined by using a scanning electron microscope (SEM; JEOL 6300) equipped with an energy-dispersive X-ray spectrometer (EDS).

Theoretical

In order to investigate the effect of the Na^+ ions at initial stages during the cobalt electrodeposition, we analyze from theoretical quantum study the redistribution of active sites on graphite surface occasioned by Na^+ adsorption process. In all calculations, we performed restricted optimizations in where the adsorption coordinates of Na^+ cation atom was optimized while the coordinates of surface atoms were fixed. In the present work, we test the ability of the recent reported PM6 method [19] to predict the adsorption geometries of Na^+ on graphite surface. We employed a cluster Beowulf with six processors of 2.4 GHz each one, with 1 GB of RAM for all calculations. These calculations were performed with the Package MOPAC2007 Linux version [20] and visualized with Spartan02 Linux version [21].

Results and discussion

Voltammetric study

The chemical composition of the deposition bath plays a very important role during the electrodeposition process. Thus, a specific chemical species in the deposition bath can induce changes in the thermodynamic and the kinetic parameters during the electrodeposition process. In previous work, it has been established that under the experimental conditions the predominant chemical species of Co(II) is the $[Co(H_2O)_6]^{2+}$ complex in where the equilibrium potential can be calculated as −0.533 V vs. Ag/AgCl(Satd KCl) [22]. Thus, under our experimental conditions, the cobalt electrodeposition process should follows the next equation:

$$\left[Co(H_2O)_6\right]^{2+} + 2e^- \rightarrow Co^0 + 6H_2O \quad (1)$$

Figure 1 shows the typical voltammetric responses, at the scan rate of 40 mV s^{-1}, obtained from GCE/10^{-2}M of $CoSO_4$+1 M Na_2SO_4 (system I) and HOPG/10^{-2}M of $CoSO_4$+1 M Na_2SO_4 (system II) systems. For both systems, note at direct scan, the formation of peaks A an A' at −0.960, −1.020 V, respectively. During the inverse of the potential scan, it is possible to observe the crossovers, E_{C1}, E_{C2} which are typical of the formation of a new phase involving a nucleation process [23]. In the anodic zone, it is possible to observe two principal peaks C and C' at around −0.240 and −0.200 V, respectively, preceded by a shoulder (B and B'). Shoulders B and B' have been associated with the dissolution of a hydrogen rich cobalt phase [24]. Note

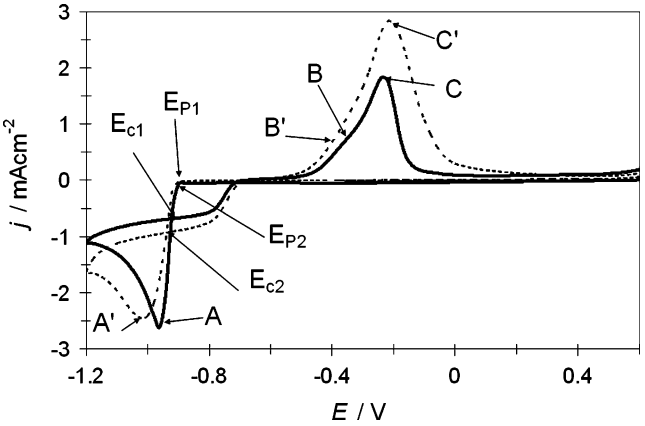

Fig. 1 A comparison of two cyclic voltammetric curves obtained in the GCE (*solid line*) and HOPG (*broken line*) from an aqueous solution 10^{-2}M of $CoSO_4$+1 M Na_2SO_4 (pH 7.1). The potential scan rate was started at 0.600 V toward the negative direction with a potential scan rate of 40 mV s^{-1}

that the shoulder corresponding to the voltammogram in system I is smaller than in system II, suggesting a lower influence of the hydrogen reduction process. It is also shown that the cobalt electrodeposition process starts at −0.900 V (E_{P1}) and −0.910 V (E_{P2}) approximately for systems I and II, respectively. Last results suggest that, energetically, the energetic cost to perform the cobalt nucleation process is similar for both systems.

Chronoamperometric study

Formation of new phases generally occurs through nucleation and growth mechanisms and the corresponding current transients can provide valuable information about the kinetics of electrodeposition. Figure 2a–b shows a set of current density transients recorded at different potentials by potential step technique from systems I and II. These transients were obtained by applying an initial potential of 0.600 V on the surface of the carbon electrode. At this potential value, the cobalt deposition had not still begun (see Fig. 1). After the application of this initial potential, a step of negative potential (E_c) was varied on the surface of the electrode for 32 s. All transients obtained exhibited a falling current at the shorter times. After this falling current, in each case, the transients showed a typical current maximum (j_m) which is characteristic of a typical three dimensional nucleation process with hemispherical diffusion control (3D-dc) of the growing crystallites [25, 26]. The decayed current recorded after the current maximum was analyzed employing the Cottrell's equation [27]. For both systems, a good description was obtained and an average value of 8.6×10^{-6}cm^2 s^{-1} for the diffusion coefficient was calculated. It is interesting to observe the strong falling currents at short times, particularly in system I (Fig. 2a). In order to elucidate the physical nature of these currents, we have carried out a comparative experiment by recording current transients under the same experimental conditions: electrodes (GCE and HOPG), initial potential, potential step, time, and temperature but in absence of Co^{2+} in the electrolyte solution, i.e., in 1 M Na_2SO_4. The results are shown in Fig. 3 a_s, b_s. The comparison with the transients obtained in a bath containing cobalt (Fig. 3 a, b) indicates that the falling currents are due to the supporting electrolyte and they cannot be associated with any cobalt reduction process. The same behavior was obtained for all experiments analyzed in this work. A similar procedure has been applied in order to analyze the electrodeposition of platinum on metallic and non-metallic substrates [28]. Although, usually the falling currents associated with the double-layer charging take tenths of milliseconds or less, it has recently been showed that a non-uniform accessibility for the surface by ions from solution may occasion that the electrode charges anomalously in response to a potential step, modifying the rate of double-layer charging [29, 30]. Thus, under our experimental conditions, it is probably because the charges trapped in the double-layer of system II may move faster than in system I interface due to that the HOPG exhibits a more uniform accessibility to the ions from solution.

A classification of the nucleation as instantaneous or progressive from transients showed in Fig. 2 is possible following the criteria established by Sharifker et al. (SM)

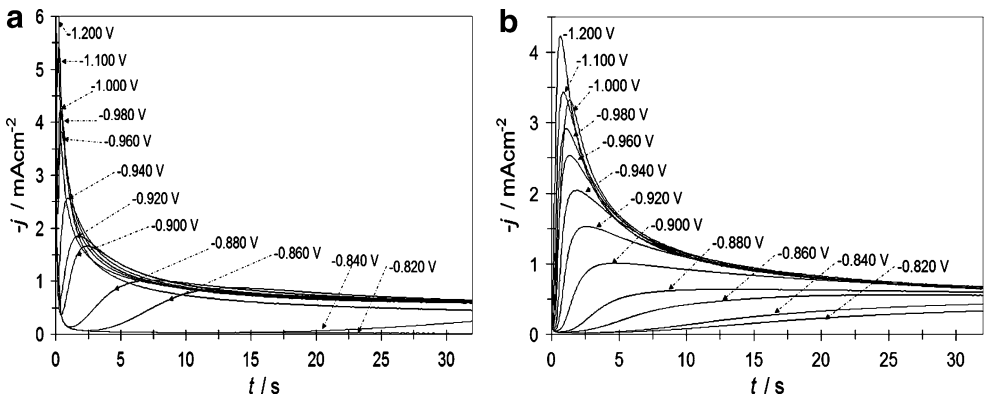

Fig. 2 A set of current transients obtained from aqueous solution 10^{-2}M of $CoSO_4$+1 M Na_2SO_4 (pH 7.1) on **a** GCE and **b** HOPG electrodes by means of the potential step technique for different potential step values (mV) indicated in the figure. In all the cases, the initial potential was 0.600 V

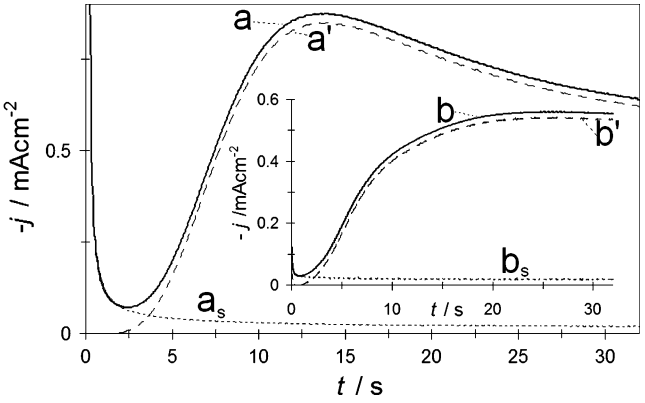

Fig. 3 Current transients obtained at −0.860 V from aqueous solution 10^{-2}M of $CoSO_4$+1 M Na_2SO_4 on **a** GCE and **b** HOPG substrates and current transients obtained at −0.860 V from aqueous solution 1 M Na_2SO_4 on GCE (a_s) and HOPG substrates (b_s). Current transients labeled as a' and b' result from the subtraction of transient a_s from transient a and b_s from transient b, respectively

[25] wherein the experimental transients in a non-dimensional form by plotting $j^2/j_m{}^2$ vs. t/t_m are compared with those theoretical generated from Eqs. (2) and (3) for instantaneous and progressive nucleation, respectively.

$$\frac{j^2}{j_m^2} = 1.9254\left(\frac{t}{t_m}\right)^{-1}\left\{1-\exp\left[-1.2564\left(\frac{t}{t_m}\right)\right]\right\}^2 \quad (2)$$

$$\frac{j^2}{j_m^2} = 1.2254\left(\frac{t}{t_m}\right)^{-1}\left\{1-\exp\left[-2.3367\left(\frac{t}{t_m}\right)^2\right]\right\}^2 \quad (3)$$

In order to identify the kind of nucleation processes involved in the present work, we perform the comparison of the theoretical dimensionless transients, generated by Eqs. (2) and (3) with the corrected experimental dimensionless current transients obtained from system I and system II. The corrected transients were obtained by subtracting, from the original transients, the current associated to the supporting electrolyte (see Fig. 3 a′–b′). Figure 4 shows this comparison; observe that for both systems, it is clear that, at initial stages, all experimental data fall within the range of validity of the theory proposed by SM [25]. However, at lower overpotentials, a deviation after the maximum was observed. It is important to mention that, from these plots, it was not possible to classify the nucleation process as instantaneous or progressive. Here, it must be reminded that the theoretical curves generated by Eqs. (2) and (3) correspond to two extreme cases of the nucleation process and in some cases a classification is not possible. Moreover, these kinds of plots have been strongly criticized by Hermann and Tarallo (HT) suggesting that such representations must be discouraged; because their utility to get qualitative conclusions is not definitive in all cases [31]. However, an additional efficacy of these plots is that if the experimental data fall within the range of validity of the theory proposed the full equation can be used to predict the overall behavior. Hermann et al. have proposed a correction to the model initially proposed by SM, wherein the deviations observed in Fig. 4 can be considered by using the following equation [32]:

$$j_{3D-dc(HT)}(t) = zFDC\frac{1}{(\pi Dt)^{1/2}}\times\frac{\phi}{\theta} \times\left[1-\exp\left(-\alpha_S N_0(\pi Dt)^{1/2}t^{1/2}\theta\right)\right] \quad (4)$$

with

$$\theta = 1-\frac{(1-\exp(-At))}{At} \quad (5)$$

$$\phi = 1-\frac{e^{-At}}{(At)^{1/2}}\int_0^{(At)^{1/2}} e^{\lambda^2}\mathrm{d}\lambda = \\ = 1-\frac{1}{(At)^{1/2}}\left(\frac{0.051314213+0.47910725(At)^{1/2}}{1-1.2068142(At)^{1/2}+1.185724(At)}\right) \quad (6)$$

where $j(t)$ is the current density, z is the number of exchanged electrons, F is the Faraday constant, α_S=2 $[2V_mDC]^{1/2}$, V_m is the molar volume of the deposit, A is the nucleation rate, and N_0 is the number density of active sites and all other parameters have their conventional meanings.

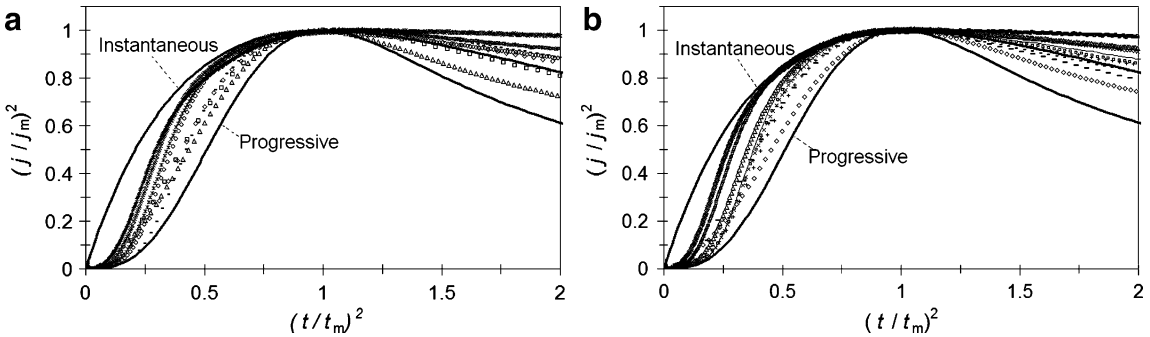

Fig. 4 Comparison of experimental transients normalized through the coordinates of its respective local maximum (t_m, j_m), with the theoretical non-dimensional curves corresponding to **a** system I and **b** system II

Thus, by using a non-linear fitting to the corrected experimental transients to the selected model, the nucleation rate, diffusion coefficient, and the number of active nucleation sites can be obtained. Figure 5 shows a typical comparison of the corrected experimental current transients for systems I and II with the theoretical one generated by non-linear fitting of experimental data to Eq. (4). It could be observed that the model expressed by Eq. (4) adequately accounted for the behavior of all experimental transients. The physical parameters obtained from the adjustments to Eq. (4) are summarized in Table 1. It was seen that an increment of the nucleation rate and the number density of active sites values was obtained when the overpotential applied was increased.

From the nucleation rates values reported in Table 1, it is possible to calculate the Gibbs free energy of nucleation as [33–35]

$$A = k_3 \exp\left(-\frac{\Delta G}{K_B T}\right) = k_3 \exp\left(\frac{k_4}{\eta^2}\right) \quad (7)$$

where ΔG is the Gibbs free energy of nucleation, J nuclei^{-1}; K_B is the Boltzmann constant (1.38066×10^{-23} J mol^{-1}), $k_3 = N_0\omega_{n_{+c}}\Gamma$ where $\omega_{n_{+c}}$ is the frequency of attachment of single atoms to the critical nucleus and Γ is the non-equilibrium Zeldovich factor and depends exponentially on the overpotential [36]. On the other hand, $k_4 = -\left(16\pi\gamma^3 M^2\phi(\theta)/3\rho^2 z^2 F^2 kT\right)$, where γ is the interfacial tension of nucleus with its mother phase, $\phi(\theta)$ is a function of the contact angle (θ) between the nucleus and the substrate, and $k = (8\pi C_0 M/\rho)^{1/2}$ [36] and all other parameters have their conventional meanings. In order to calculate the value of Gibbs free energy of nucleation from experimental transients, an ln A vs. η^{-2} plot can be constructed according to Eq. (7), and then from the slope k_4 of the observed linear relationship, ΔG could be calculated at each particular overpotential by using Eq. (8):

$$\left(-\frac{\Delta G}{K_B T}\right) = \frac{k_4}{\eta^2} \quad (8)$$

where T is the absolute temperature, K. Figure 6 shows a linear tendency between ln A vs. η^{-2} giving a slope of −8.5 and −4.3 for systems I and II. The average ΔG calculated with these slopes were 1.97×10^{-20} J nuclei^{-1} and 3.58×10^{-20} J nuclei^{-1} for system I and system II, respectively. The ΔG values obtained are of the same order of magnitude as the value obtained for the electrocrystallization of Ni on carbon microelectrodes [37] and copper sulfide on copper [38]. These energies correspond to the ΔG value requirements for the stable nucleus formation [29, 30]. It is clear that cobalt electrodeposition process is

Table 1 Potential dependence for the nucleation parameters during cobalt electrodeposition on carbon electrodes

−E (V)	GCE			HOPG		
	A (s^{-1} cm^{-2})	D 10^5 (cm^2 s^{-1})	N_0 10^{-6} (cm^2)	A (s^{-1} cm^{-2})	D 10^5 (cm^2 s^{-1})	N_0 10^{-6} (cm^2)
0.840	0.25	0.73	0.78	0.21	1.47	0.06
0.860	0.45	0.73	0.78	0.32	0.87	0.21
0.880	0.76	0.78	0.82	0.38	0.83	0.31
0.900	1.13	0.68	2.93	0.48	0.89	0.66
0.920	1.49	0.68	3.66	0.61	0.91	1.49
0.940	2.59	0.63	7.87	0.74	1.00	2.33
0.960	4.46	0.58	18.71	0.90	0.99	3.56
0.980	5.98	0.58	22.86	1.00	1.00	4.69
1.000	8.50	0.59	37.07	1.30	0.99	7.21
1.100	36.60	0.53	149.37	2.51	1.00	11.29
1.200	120.23	0.59	928.20	4.48	1.01	12.06

The values were obtained from best-fit parameters found through the fitting process of the experimental j–t plots using Eq. (4)

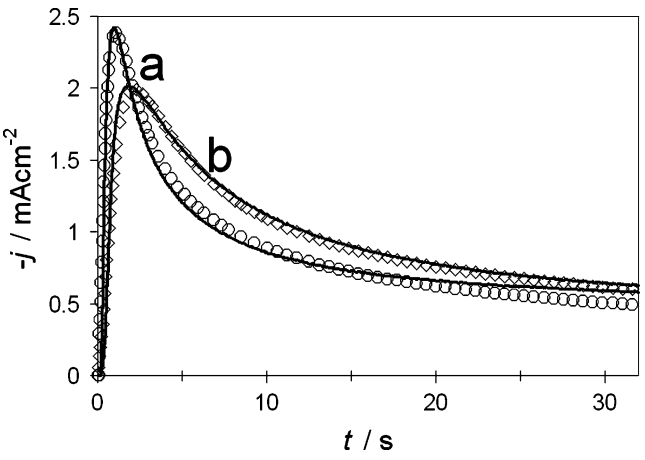

Fig. 5 Comparison between an experimental corrected current density transient (—) recorded during cobalt electrodeposition onto GCE (*a*) and HOPG (*b*) electrodes when a potential value of −0.940 V was applied with a theoretical transient (O, GCE) and (Δ,HOPG) generated by non-linear fitting of Eq. (4)

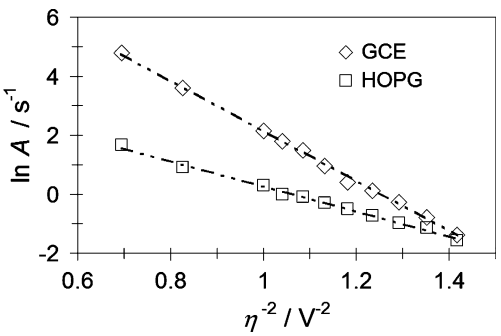

Fig. 6 ln A vs. η^{-2} plot, used to calculate the Gibbs energy of nucleation according to Eq. (7). The *broken straight line* corresponds to the linear fit of the experimental data

slightly more favored on the GCE substrate, probably because there are more structural defects that favor the nucleation process. However, if one employs these averages ΔG to calculate the critical cobalt nucleus (n_c) according to the classical formula $n_c=2\Delta G/ze_0\eta$ at −0.880 V for example, the results obtained are 0.139 and 0.254 atoms, which cannot be possible. Thus, it is better to estimate the critical size of the cobalt nucleus in the framework of the atomistic theory of electrolytic nucleation through the following equation [39]:

$$n_c = \left(\frac{k_B T}{ze_0}\right)\left(\frac{\mathrm{d}\ln A}{\mathrm{d}\eta}\right) - \alpha_{Co} \tag{9}$$

where α_{Co} is the transfer coefficient for cobalt reduction. The plots ln A vs. η showed a linear tendency as depicted in Fig. 7. The values of d(ln A)/d(E) were 16.5 and 8.6 for systems I and II, respectively; thus, in both substrates, the critical cluster's size calculated was $n_c=0$. This value means that each active site is a critical nucleus.

Through the physical constants reported in Table 1, it was also possible to calculate the saturation number of nuclei (N_s). This estimation was made using Eq. (10) [25]:

$$N_s = \left(\frac{AN_0}{2kD}\right)^{1/2} \tag{10}$$

For systems I and II, the results obtained for N_s, employing the data shown in Table 1, are summarized in Table 2. Observe that the N_s values increased with the applied potential. It is important to mention that, due to the exclusion zones of the deposit, caused by the hemispherical diffusional gradients of 3D nucleus, the N_s will be always lower than the N_0 values in the same applied potential, and both grow in accordance with a more negative potential. Analyzing the N_s/N_0 ratio, this value was small (lower than 0.2 in most of the cases) for both systems. This result suggested that the cobalt electrodeposition was not favored in all initially available sites. The reason for this behavior could be the conversion of sites into growing nuclei, and because nucleation was confined to those active centers that have not been included within an exclusion zone, enhanced by the concentration depletion around centers growing under mass-transfer control in the vicinity of each nucleus [24].

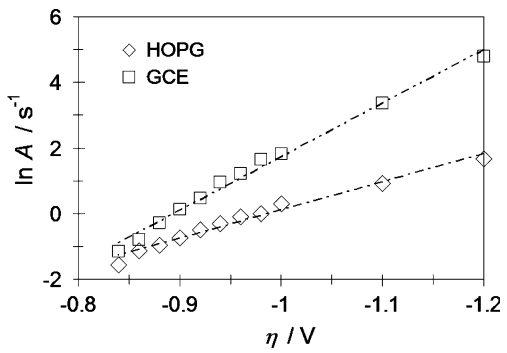

Fig. 7 ln A vs. η plot, used to calculate the critical nuclei's size according to Eq. (9). The *broken straight line* corresponds to the linear fit of the experimental data

Table 2 Potential dependence of N_s from system I and system II calculated from physical constants showed in Table 1 and Eq. (10)

−E (V)	GCE N_s 10^{-6} (cm^2)	HOPG N_s 10^{-6} (cm^2)
0.840	0.102	0.018
0.860	0.136	0.054
0.880	0.177	0.073
0.900	0.435	0.118
0.920	0.559	0.196
0.940	1.122	0.258
0.960	2.352	0.355
0.980	3.013	0.426
1.000	4.543	0.607
1.100	19.935	1.049
1.200	85.319	1.438

Morphological analysis

The morphology of the electrodeposits was studied by scanning electron microscopy (SEM). SEM micrographs of the electrodeposit formed potentiostatically, at −0.940 V, are shown in Fig. 8. The deposit consisted of dispersed particles with spherical microstructure in both systems. It is possible to observe that on GCE, Fig. 8a–b, a major amount of nuclei was obtained with respect to HOPG substrate (see Fig. 8c–d); however, the same nuclei's size (~1 μm) was obtained in both cases. At −1.100 V, Fig. 9, the deposits were more compact with a finer grain size. The increase in the nuclei number at −1.100 V probably is due to the increase of the active nucleation sites with the potential applied. Also, observe that at −1.100 V the nuclei's size was similar in both substrates. These facts suggest that, at same overpotential, the nuclei size is independent of the carbon substrate employed and the kind of carbon substrate affects only their number. If one compares the nuclei's size at the two overpotentials, it is possible to note at −1.100 V that the growth rate of the cobalt clusters diminishes when their number increases, probably due to the strongly reduced concentration of cobalt ions when they are consumed by a larger number of growing particles. If one counts the number of nuclei in Fig. 8, there are 65 nuclei for GCE and 18 for HOPG, the ratio is 3.6 which is very close to 3.4 which was obtained from Table 2 as $N_{0,GCE}/N_{0,HOPG}$ at −0.940 V. Last results indicate a good concordance between the microscopic study and the one predicted by

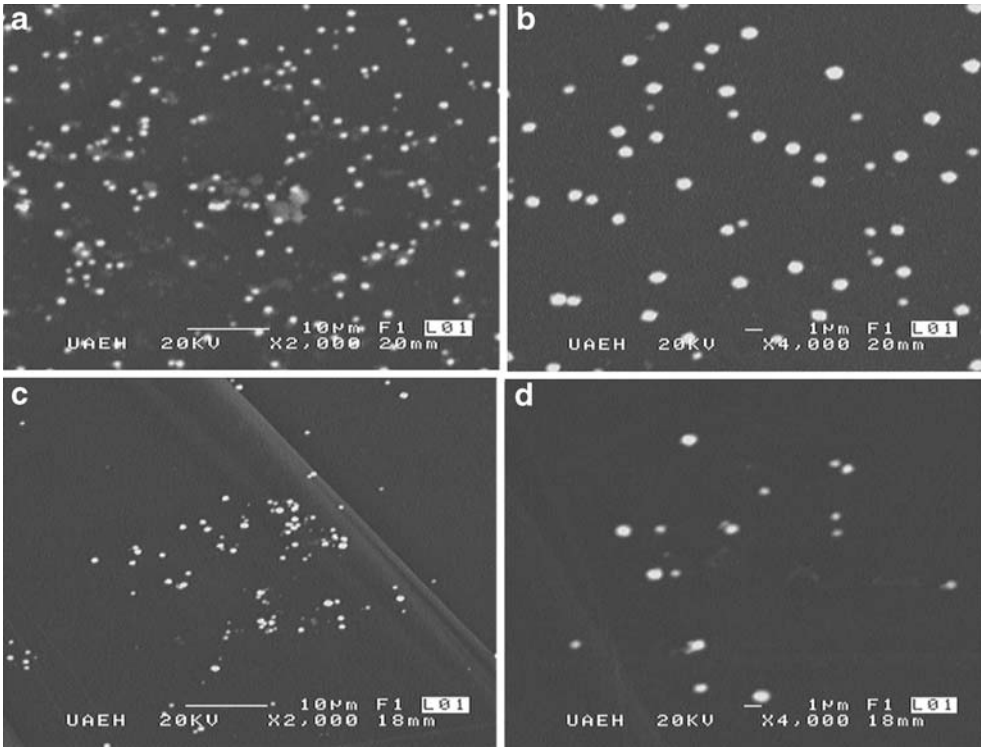

Fig. 8 SEM images of the deposits obtained at −0.940 V on **a** GCE and **b** HOPG, from an aqueous solution 10^{-2}M of $CoSO_4$+1 M Na_2SO_4 (pH 7.1). 2,000× and 4,000× magnification were used

Eq. (4). In order to verify that the nuclei showed in Figs. 8 and 9 correspond to cobalt element, we carried out an EDS analysis of these grains. Figure 10 shows the general EDS spectrum obtained in all cases, confirming the cobalt presence.

Theoretical quantum study

It has been reported that Na^+ ions do not react electrochemically at the electrode surface allowing a major control on the electrodeposition [18]. However, it is well known that an adsorption process can modify the electronic structure of the substrate in its reactivity. In order to analyze the influence of Na^+ adsorption process on carbon surface reactivity; we performed a theoretical quantum study to determine this effect. A good parameter to analyze the reactivity is to determine the number and distribution of active sites on a surface, wherein these can be calculated from conceptual density functional theory (DFT). In this context, Parr and Yang showed that sites in chemical species with the largest values of Fukui's Function ($f(r)$) are those with higher reactivity, where the Fukui's function is defined as [40]:

$$f(r) = \left(\frac{\partial \rho(r)}{\partial N}\right)_v, \tag{11}$$

where ρ is the electronic density, N is the number of electrons, and v is the external potential exerted by the nucleus. Fukui's function can be evaluated through the frontier orbital within the *frozen core* approximation. This

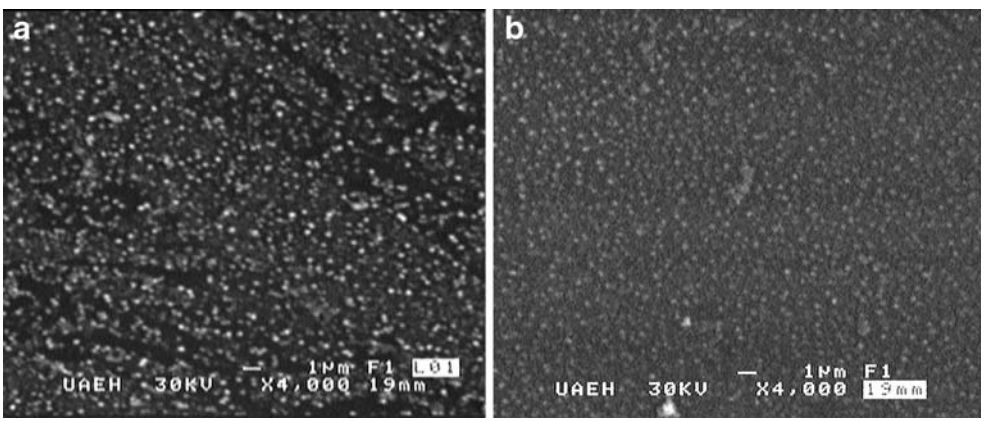

Fig. 9 SEM images of the deposits obtained at −1.100 V on **a** GCE and **b** HOPG, from an aqueous solution 10^{-2}M of $CoSO_4$+1 M Na_2SO_4 (pH 7.1). 4,000× magnification was used

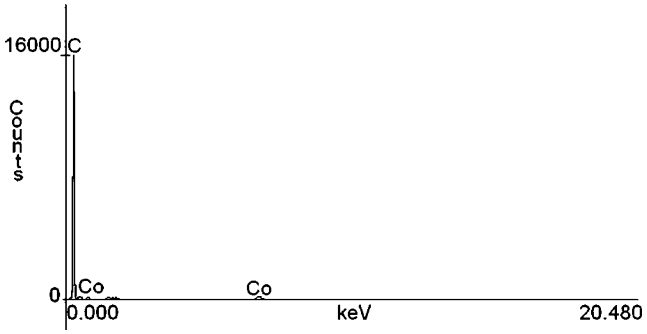

Fig. 10 The EDS analysis reveals the presence of Co in the aggregates

approximation considers that when there is a variation on the number of electrons, the respective frontier orbital is only affected, thus when N increases to $N+\mathrm{d}N$ [40]:

$$f^{-}(r) \cong \phi_{\mathrm{H}}^{*}(r)\phi_{\mathrm{H}}(r) = \rho_{\mathrm{H}}(r), \tag{12}$$

Where $\rho_{\mathrm{H}}(r)$ is the electron density of the highest occupied molecular orbital (HOMO). $f^{-}(r)$ gives us the more feasible sites (at the reference molecule) to an electrophilic attack.

On the other hand, the study of the electronic properties of the some surfaces still is difficult. Additionally, if one studies the nucleation process from an electronic point of view by employing quantum theories, one must consider that this process occurs preferentially on those active sites that have the highest surface energy. However, at electronic level, to analyze the structural defects on a surface requires a big surface model, which become prohibitive in common workstations. Thus, a common skill to analyze the surface phenomena is to consider that this kind of processes are occurring at local level; under this consideration, it is possible to analyze the effect only in a small region, since the results will be valid only at closer sites where the process is studied. Therefore, new methods and skills are required in order to handle main-group elements as well as solids. Recently, the semi-empirical method PM6 developed by Stewart's group offers new possibilities to model reactions at solid state at common workstations [19]. For the case of graphite, it has been reported that a PM6 calculation predicts that the structure would be essentially the same as that given by DFT methods [41]. Additionally, our experimental results suggest that the nucleation process is similar on GCE and HOPG by this reason; at present work, we use these capabilities of PM6 method to determine the reactivity changes on HOPG surface. Only Na^{+} effect was studied because, during reduction process, a negative polarization is expected on electrode surface. Thus, cation adsorption should be increased with respect to the anion adsorption. Thus, if one considers that the concentration of Na^{+} in the solution is 1.0 M with respect to the 0.01 M of cobalt, then at initial stages the Na^{+} adsorption process should be favored.

Distribution of the electrophilic active sites on HOPG surface

HOPG surface was modeled as a finite graphite layer (Fig. 11a) while the adsorption process of Na^{+} on graphite is modeled as shown in Fig. 11b. It is important to mention that, in a finite cluster size, the frontier effects can produce an artificial reactivity on the borders. There are two possible ways to take into account the border effects into the calculations; one way consists in increasing the cluster size until the electronic properties do not change in the center of the cluster. A second way consists in saturating the valences on the borders of the cluster considering, in an artificial way, the effect of the other atoms in the limits of the system. We decided to analyze it by employing the second way. To study the adsorption process of Na^{+}, in a first step, we need to identify the electrophilic sites on HOPG surface where their distribution can be derived from Eq. (12). In order to determine this distribution, we analyze

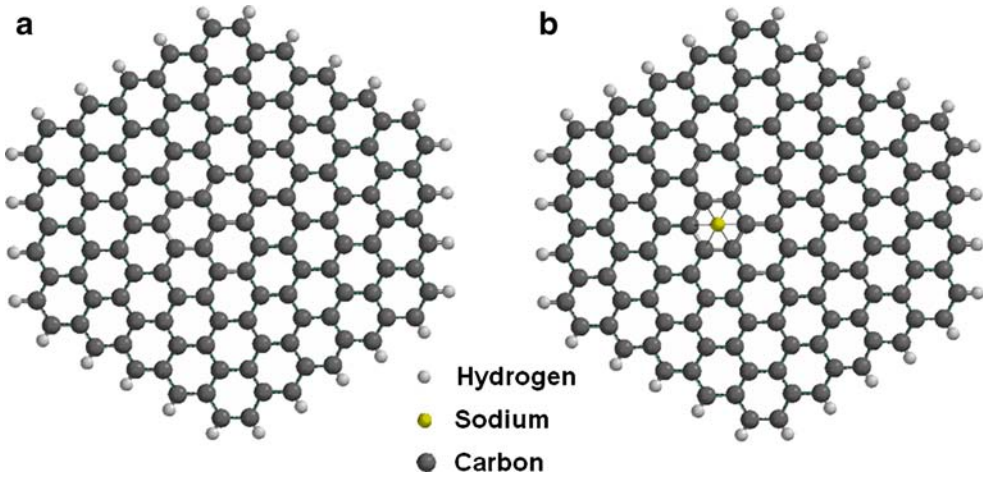

Fig. 11 Clusters models. **a** HOPG surface (158 atoms), **b** Na^{+} adsorbed on HOPG surface (159 atoms)

the sites where the HOMO frontier orbital attains its larger absolute value on the surface for each one of the studied clusters. The ground state HOMO (absolute value) for the cluster shown in Fig. 11a, with charge=0, is mapped onto a density isosurface (with a value equal to 0.002 e a.u.$^{-3}$; Fig. 12a). The color code indicates the HOMO's values along this surface. So the darker zones (blue zones) indicate sites amenable for easier attack by charge acceptors while the lighter regions (red zones) indicate predominant attack by charge donors. Also, note that there are nodal zones where the charge donors might attack. These nodal zones suggest a possible path of movement of the charge donor, which might describe species that undergo diffusion on the surface because there are similar energetic situations [42]. From Fig. 12a, it is possible to observe a periodical distribution of the electrophilic active sites in the center of the cluster located at hollow positions. This distribution suggests that a charge acceptor might be adsorbed on hollow positions; it is the center of the ring. If one applies a potential on electrode surface, a charge redistribution is expected where such redistribution modifies the electronic structure changing the surface reactivity. We analyze this effect modifying the charge on the model. In Fig. 12b–d is depicted the behavior obtained for graphite surface at different charge values. It is interesting to note that the number and position of active sites increases with the cluster's charge; however, from −2, the distribution of active sites is constant, which indicates that this behavior should be kept at lower overpotentials.

HOMO mapped onto a density isosurface of the optimized structures with the Na^+ cation on HOPG at different charges are shown in Fig. 12e–h. Observe that the Na^+ adsorbed modify the distribution of the electrophilic actives sites. It is possible to note that Na^+ adsorbed diminish the reactivity of the surface in closer sites and the last effect is increased when the negative charge is lower in the cluster. Thus, it is possible to suggest that, if Na^+ adsorption process occurs, Co^{2+} cation must be adsorbed out of the influence zone of the Na^+; occasionating a disperse cobalt nucleation process on HOPG surface. Indeed, these results agree with the observed from SEM images on GCE and HOPG electrodes.

Conclusions

We have studied the cobalt electrodeposition from 10^{-2}M $CoSO_4$, 1 M Na_2SO_4 aqueous solutions on GCE and HOPG electrodes. The result showed that electrodeposition of cobalt is a diffusion-controlled process with a typical 3D nucleation mechanism in both substrates. The average ΔG calculated for the stable nucleus formation were 1.97×10^{-20}J nuclei^{-1} and 3.58×10^{-20}J nuclei^{-1} for system I and system II, respectively. The morphological analysis indicated, at same overpotential, similar nucleation and growth processes on carbon substrates. The nuclei's size obtained was dependent of the overpotential applied; at lower overpotentials, the growth rate of the cobalt clusters diminishes when their number increases probably due to the strongly reduced concentration of cobalt ions when they are consumed by a larger number of growing particles, allowing the formation of smaller nuclei than those obtained at higher overpotentials. The semi-empirical study

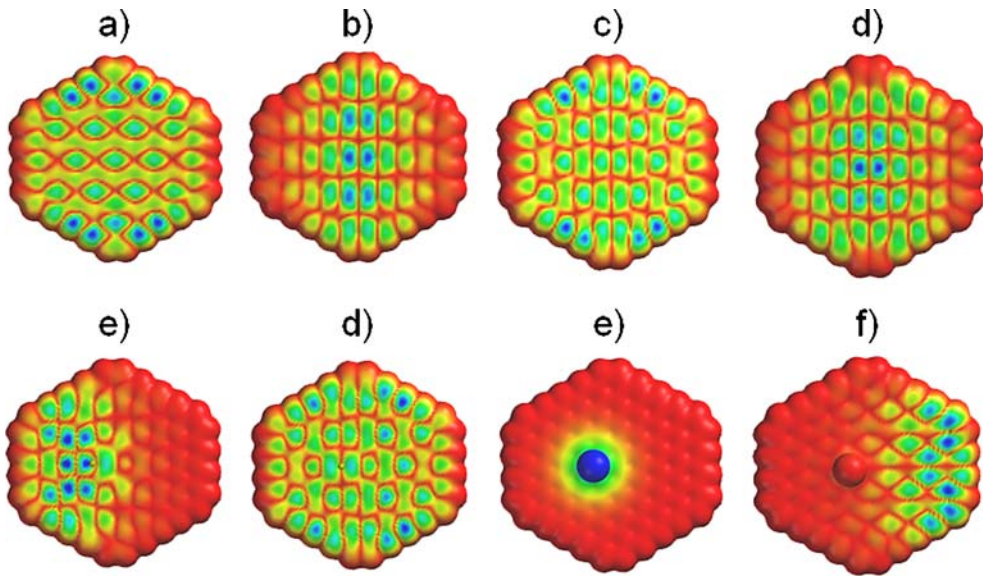

Fig. 12 Mapping of the HOMO of structures optimized at PM6 level onto a density isosurface (value ρ=0.002 e a.u.$^{-3}$). *Lighter zones* (*red zones*) have the lower value of HOMO, and *darker zones* (*blue zones*) have the higher one. The charge used were **a** 0, **b** −1, **c** −2, **d** −3, **e** 0, **f** −1, **g** −2, and **h** −3

showed that Na^+ adsorbed on HOPG surface inhibits the reactivity of the HOPG in closer sites to the adsorption site favoring the formation of disperse cobalt clusters on carbon electrodes.

Acknowledgments C.H.R.R. is grateful for a graduate student fellowship from CONACyT. We gratefully acknowledge financial support from CONACyT project APOY-COMPL-2008 No. 91261 and to the Universidad Autónoma del Estado de Hidalgo. M.R. acknowledges financial support from DGAPA-PAPIIT, project number IN-112106. Authors acknowledge Juan Hernandez for the SEM technical assistance. We acknowledge Professors M.E. Palomar-Pardavé and M. Romero-Romo for fruitful discussions. We are also grateful to the reviewers of the manuscript for valuable suggestions.

References

1. Su JL, Chen MM, Lo J, Lee RE (1988) J Appl Phys 63:4022. doi:10.1063/1.340536
2. Quinn HF, Croll IM (1980) Advances in X-ray analysis. Plenum, New York
3. Grujicic D, Pesic B (2004) Electrochim Acta 49:4719. doi:10.1016/j.electacta.2004.05.028
4. Rehim SSAE, Wahaab SMAE, Ibrahim MAM, Dankeria MA (1998) J Chem Technol Biotechnol 73:369. doi:10.1002/(SICI)1097-4660(199812)73:4<369::AID-JCTB971>;3.0.CO;2-P
5. Gomez E, Valles E (2002) J Appl Electrochem 32:693. doi:10.1023/A:1020194532136
6. Floate S, Hyde M, Compton RG (2002) J Electroanal Chem 523:49. doi:10.1016/S0022-0728(02)00709-X
7. Gomez E, Marin M, Sanz F, Valles E (1997) J Electroanal Chem 422:139. doi:10.1016/S0022-0728(96)04899-1
8. Soto AB, Arce EM, Palomar-Pardave M, Gonzalez I (1996) Electrochim Acta 41:2647. doi:10.1016/0013-4686(96) 00088-6
9. Myung N, Ryu KH, Sumodjo PTA, Nobe K (1998) Fundamental aspects of electrochemical deposition and dissolution including modeling. Electrochemical Society, Pennington
10. Palomar-Pardave M, González I, Soto AB, Arce EM (1998) J Electroanal Chem 443:125. doi:10.1016/S0022-0728(97)00496-8
11. Mendoza-Huizar LH, Robles J, Palomar-Pardavé M (2002) J Electroanal Chem 521:95. doi:10.1016/S0022-0728(02)00659-9
12. Cui CQ, Jiang SP, Tseung ACC (1990) J Electrochem Soc 137 (11):3418. doi:10.1149/1.2086232
13. Nakano H, Nakahara K, Kawano S, Oue S, Akiyama T, Fukushima H (2002) J Appl Electrochem 32:43. doi:10.1023/A:1014219106152
14. Fletcher S, Halliday CS, Gates D, Westcott, Liwin T, Nelson G (1983) J Electroanal Chem 159:267. doi:10.1016/S0022-0728(83)80627-5
15. Rehim SSAE, Ibrahim MAM, Dankeria MM (2002) J Appl Electrochem 32:1019. doi:10.1023/A:1020945031502
16. Wheeler DR, Wang JX, Adžić RR (1995) J Electroanal Chem 387:115. doi:10.1016/0022-0728(95)03864-D
17. Jia-Wei Y, Jian-Ming W, Wu Q, Zhao-Xiong X, Bing-Wei M (2003) Langmuir 19:7948. doi:10.1021/la034500s
18. Rivera M, Rios-Reyes CH, Mendoza-Huizar LH (2008) Appl Surf Sci 255:1754. doi:10.1016/j.apsusc.2008.06.016
19. Stewart JJP (2007) J Mol Model 13:1173. doi:10.1007/s00894-007-0233-4
20. Stewart JJP (2008) MOPAC2007 Version 8.032L. Stewart Computational Chemistry, Colorado Springs
21. Wavefunction (2002) Spartan'02 for Linux package. Wavefunction Inc., Irvine
22. Rios-Reyes CH, Rivera M, Mendoza-Huizar LH (2008) Electrochemical and AFM study of cobalt electrodeposits from sodium and ammonium sulfate solutions onto HOPG electrode. In: Mendoza-Huizar LH (ed) Theoretical and experimental advances in electrodeposition. Research SignPost, Trivandrum
23. Greef R, Peat R, Peter LM, Pletcher D, Robinson J (1985) Instrumental methods in electrochemistry. Ellis Horwood, Chichester
24. Palomar-Pardave M, Gonzalez I, Soto AB, Arce EM (1998) J Electroanal Chem 443:125. doi:10.1016/S0022-0728(97)00496-8
25. Scharifker BR, Hills G (1983) Electrochim Acta 28:879. doi:10.1016/0013-4686(83)85163-9
26. Scharifker BR, Mostany J (1984) J Electroanal Chem 177:13. doi:10.1016/0022-0728(84)80207-7
27. Bard AJ, Faulkner LR (2001) Electrochemical methods. Fundamental and applications. Wiley, New York
28. Stoychev D, Papoutsis A, Kelaidopoulou A, Kokkinidis G, Milchev A (2001) Mater Chem Phys 72:360. doi:10.1016/S0254-0584(01)00337-6
29. Myland JC, Oldham KB (2005) J Electroanal Chem 575:81. doi:10.1016/j.jelechem.2004.09.004
30. Zhu CY, Wu R, Wu YQ, Fan YL, Jiang ZM, Yang XJ (2007) Nanotechnology 18:235403. doi:10.1088/0957-4484/18/23/235403
31. Hermann L, Tarallo A (2000) Electrochem Commun 2:85. doi:10.1016/S1388-2481(99)00144-7
32. Hermann L, Tarallo A (1999) J Electroanal Chem 470:70. doi:10.1016/S0022-0728(99)00221-1
33. Southampton Electrochemistry Group (1985) Instrumental methods in electrochemistry. Wiley, New York
34. Mostany J, Mozota J, Scharifker BR (1984) J Electroanal Chem 177:25. doi:10.1016/0022-0728(84)80208-9
35. Serruya A, Mostany J, Scharifker BR (1999) J Electroanal Chem 464:39. doi:10.1016/S0022-0728(98)00464-1
36. Milchev A (2002) Electrocrystallization: fundamentals of nucleation and growth. Kluwer, Norwell
37. Petrović Ž, Metikoš-Huković M, Grubač Z, Omanović S (2006) Thin Solid Films 513:193. doi:10.1016/j.tsf.2006.01.026
38. Scharifker B, Rugeles R, Mozota J (1984) Electrochim Acta 29:261. doi:10.1016/0013-4686(84)87057-7
39. Milchev A (1991) J Contemp Phys 32:321. doi:10.1080/00107519108223705
40. Parr RG, Yang W (1989) Density-functional theory of atoms and molecules. Oxford University Press, New York
41. Bucknum MJ, Pickard CJ, Stamatin I, Castro EA (2006) J Theor Comput Chem 5:175. doi:10.1142/S0219633606002209
42. Mendoza-Huizar LH, Palomar-Pardave ME, Robles J (2004) J Mol Struct 679:187